$D^{*\pm}$ Meson Production in Deep–Inelastic Diffractive Interactions at HERA

H1 Collaboration

Abstract

A measurement is presented of the cross section for $D^{*\pm}$ meson production in diffractive deep–inelastic scattering for the first time at HERA. The cross section is given for the process $ep \rightarrow eXY$, where the system X contains at least one $D^{*\pm}$ meson and is separated by a large rapidity gap from a low mass proton remnant system Y. The cross section is presented in the diffractive deep–inelastic region defined by $2 < Q^2 < 100$ GeV^2, $0.05 < y < 0.7$, $x_{I\!P} < 0.04$, $M_Y < 1.6$ GeV and $|t| < 1$ GeV^2. The $D^{*\pm}$ mesons are restricted to the range $p_{T,D^*} > 2$ GeV and $|\eta_{D^*}| < 1.5$. The cross section is found to be $246 \pm 54 \pm 56$ pb and forms about 6% of the corresponding inclusive $D^{*\pm}$ cross section. The cross section is presented as a function of various kinematic variables, including $z_{I\!P}^{obs}$ which is an estimate of the fraction of the momentum of the diffractive exchange carried by the parton entering the hard-subprocess. The data show a large component of the cross section at low $z_{I\!P}^{obs}$ where the contribution of the Boson–Gluon–Fusion process is expected to dominate. The data are compared with several QCD–based calculations.

C. Adloff[33], V. Andreev[24], B. Andrieu[27], T. Anthonis[4], V. Arkadov[35], A. Astvatsatourov[35],
A. Babaev[23], J. Bähr[35], P. Baranov[24], E. Barrelet[28], W. Bartel[10], P. Bate[21], J. Becker[37],
A. Beglarian[34], O. Behnke[13], C. Beier[14], A. Belousov[24], T. Benisch[10], Ch. Berger[1],
T. Berndt[14], J.C. Bizot[26], J. Boehme, V. Boudry[27], W. Braunschweig[1], V. Brisson[26],
H.-B. Bröker[2], D.P. Brown[10], W. Brückner[12], D. Bruncko[16], J. Bürger[10], F.W. Büsser[11],
A. Bunyatyan[12,34], A. Burrage[18], G. Buschhorn[25], L. Bystritskaya[23], A.J. Campbell[10],
J. Cao[26], S. Caron[1], F. Cassol-Brunner[22], D. Clarke[5], B. Clerbaux[4], C. Collard[4],
J.G. Contreras[7,41], Y.R. Coppens[3], J.A. Coughlan[5], M.-C. Cousinou[22], B.E. Cox[21],
G. Cozzika[9], J. Cvach[29], J.B. Dainton[18], W.D. Dau[15], K. Daum[33,39], M. Davidsson[20],
B. Delcourt[26], N. Delerue[22], R. Demirchyan[34], A. De Roeck[10,43], E.A. De Wolf[4],
C. Diaconu[22], J. Dingfelder[13], P. Dixon[19], V. Dodonov[12], J.D. Dowell[3], A. Droutskoi[23],
A. Dubak[25], C. Duprel[2], G. Eckerlin[10], D. Eckstein[35], V. Efremenko[23], S. Egli[32], R. Eichler[36],
F. Eisele[13], E. Eisenhandler[19], M. Ellerbrock[13], E. Elsen[10], M. Erdmann[10,40,e], W. Erdmann[36],
P.J.W. Faulkner[3], L. Favart[4], A. Fedotov[23], R. Felst[10], J. Ferencei[10], S. Ferron[27],
M. Fleischer[10], Y.H. Fleming[3], G. Flügge[2], A. Fomenko[24], I. Foresti[37], J. Formánek[30],
G. Franke[10], E. Gabathuler[18], K. Gabathuler[32], J. Garvey[3], J. Gassner[32], J. Gayler[10],
R. Gerhards[10], C. Gerlich[13], S. Ghazaryan[4,34], L. Goerlich[6], N. Gogitidze[24], M. Goldberg[28],
C. Grab[36], H. Grässler[2], T. Greenshaw[18], G. Grindhammer[25], T. Hadig[13], D. Haidt[10],
L. Hajduk[6], J. Haller[13], W.J. Haynes[5], B. Heinemann[18], G. Heinzelmann[11],
R.C.W. Henderson[17], S. Hengstmann[37], H. Henschel[35], R. Heremans[4], G. Herrera[7,44],
I. Herynek[29], M. Hildebrandt[37], M. Hilgers[36], K.H. Hiller[35], J. Hladký[29], P. Höting[2],
D. Hoffmann[22], R. Horisberger[32], S. Hurling[10], M. Ibbotson[21], Ç. İşsever[7], M. Jacquet[26],
M. Jaffre[26], L. Janauschek[25], X. Janssen[4], V. Jemanov[11], L. Jönsson[20], C. Johnson[3],
D.P. Johnson[4], M.A.S. Jones[18], H. Jung[20,10], D. Kant[19], M. Kapichine[8], M. Karlsson[20],
O. Karschnick[11], F. Keil[14], N. Keller[37], J. Kennedy[18], I.R. Kenyon[3], S. Kermiche[22],
C. Kiesling[25], P. Kjellberg[20], M. Klein[35], C. Kleinwort[10], T. Kluge[1], G. Knies[10], B. Koblitz[25],
S.D. Kolya[21], V. Korbel[10], P. Kostka[35], S.K. Kotelnikov[24], R. Koutouev[12], A. Koutov[8],
H. Krehbiel[10], J. Kroseberg[37], K. Krüger[10], A. Küpper[33], T. Kuhr[11], T. Kurča[16], R. Lahmann[10],
D. Lamb[3], M.P.J. Landon[19], W. Lange[35], T. Laštovička[30,35], P. Laycock[18], E. Lebailly[26],
A. Lebedev[24], B. Leißner[1], R. Lemrani[10], V. Lendermann[7], S. Levonian[10], M. Lindstroem[20],
B. List[36], E. Lobodzinska[10,6], B. Lobodzinski[6,10], A. Loginov[23], N. Loktionova[24],
V. Lubimov[23], S. Lüders[36], D. Lüke[7,10], L. Lytkin[12], H. Mahlke-Krüger[10], N. Malden[21],
E. Malinovski[24], I. Malinovski[24], R. Maraček[25], P. Marage[4], J. Marks[13], R. Marshall[21],
H.-U. Martyn[1], J. Martyniak[6], S.J. Maxfield[18], D. Meer[36], A. Mehta[18], K. Meier[14],
A.B. Meyer[11], H. Meyer[33], J. Meyer[10], P.-O. Meyer[2], S. Mikocki[6], D. Milstead[18],
T. Mkrtchyan[34], R. Mohr[25], S. Mohrdieck[11], M.N. Mondragon[7], F. Moreau[27], A. Morozov[8],
J.V. Morris[5], K. Müller[37], P. Murín[16,42], V. Nagovizin[23], B. Naroska[11], J. Naumann[7],
Th. Naumann[35], G. Nellen[25], P.R. Newman[3], T.C. Nicholls[5], F. Niebergall[11], C. Niebuhr[10],
O. Nix[14], G. Nowak[6], J.E. Olsson[10], D. Ozerov[23], V. Panassik[8], C. Pascaud[26], G.D. Patel[18],
M. Peez[22], E. Perez[9], J.P. Phillips[18], D. Pitzl[10], R. Pöschl[26], I. Potachnikova[12], B. Povh[12],
K. Rabbertz[1], G. Rädel[1], J. Rauschenberger[11], P. Reimer[29], B. Reisert[25], D. Reyna[10],
C. Risler[25], E. Rizvi[3], P. Robmann[37], R. Roosen[4], A. Rostovtsev[23], S. Rusakov[24], K. Rybicki[6],
D.P.C. Sankey[5], J. Scheins[1], F.-P. Schilling[10], P. Schleper[10], D. Schmidt[33], D. Schmidt[10],
S. Schmidt[25], S. Schmitt[10], M. Schneider[22], L. Schoeffel[9], A. Schöning[36], T. Schörner[25],
V. Schröder[10], H.-C. Schultz-Coulon[7], C. Schwanenberger[10], K. Sedlák[29], F. Sefkow[37],
V. Shekelyan[25], I. Sheviakov[24], L.N. Shtarkov[24], Y. Sirois[27], T. Sloan[17], P. Smirnov[24],

1

Y. Soloviev[24], D. South[21], V. Spaskov[8], A. Specka[27], H. Spitzer[11], R. Stamen[7], B. Stella[31],
J. Stiewe[14], U. Straumann[37], M. Swart[14], M. Taševský[29], V. Tchernyshov[23],
S. Tchetchelnitski[23], G. Thompson[19], P.D. Thompson[3], N. Tobien[10], D. Traynor[19], P. Truöl[37],
G. Tsipolitis[10,38], I. Tsurin[35], J. Turnau[6], J.E. Turney[19], E. Tzamariudaki[25], S. Udluft[25],
M. Urban[37], A. Usik[24], S. Valkár[30], A. Valkárová[30], C. Vallée[22], P. Van Mechelen[4],
S. Vassiliev[8], Y. Vazdik[24], A. Vichnevski[8], K. Wacker[7], R. Wallny[37], B. Waugh[21], G. Weber[11],
M. Weber[14], D. Wegener[7], C. Werner[13], M. Werner[13], N. Werner[37], G. White[17], S. Wiesand[33],
T. Wilksen[10], M. Winde[35], G.-G. Winter[10], Ch. Wissing[7], M. Wobisch[10], E.-E. Woehrling[3],
E. Wünsch[10], A.C. Wyatt[21], J. Žáček[30], J. Zálešák[30], Z. Zhang[26], A. Zhokin[23], F. Zomer[26],
J. Zsembery[9], and M. zur Nedden[10]

[1] I. Physikalisches Institut der RWTH, Aachen, Germany[a]
[2] III. Physikalisches Institut der RWTH, Aachen, Germany[a]
[3] School of Physics and Space Research, University of Birmingham, Birmingham, UK[b]
[4] Inter-University Institute for High Energies ULB-VUB, Brussels; Universitaire Instelling Antwerpen, Wilrijk; Belgium[c]
[5] Rutherford Appleton Laboratory, Chilton, Didcot, UK[b]
[6] Institute for Nuclear Physics, Cracow, Poland[d]
[7] Institut für Physik, Universität Dortmund, Dortmund, Germany[a]
[8] Joint Institute for Nuclear Research, Dubna, Russia
[9] CEA, DSM/DAPNIA, CE-Saclay, Gif-sur-Yvette, France
[10] DESY, Hamburg, Germany
[11] II. Institut für Experimentalphysik, Universität Hamburg, Hamburg, Germany[a]
[12] Max-Planck-Institut für Kernphysik, Heidelberg, Germany
[13] Physikalisches Institut, Universität Heidelberg, Heidelberg, Germany[a]
[14] Kirchhoff-Institut für Physik, Universität Heidelberg, Heidelberg, Germany[a]
[15] Institut für experimentelle und Angewandte Physik, Universität Kiel, Kiel, Germany
[16] Institute of Experimental Physics, Slovak Academy of Sciences, Košice, Slovak Republic[e,f]
[17] School of Physics and Chemistry, University of Lancaster, Lancaster, UK[b]
[18] Department of Physics, University of Liverpool, Liverpool, UK[b]
[19] Queen Mary and Westfield College, London, UK[b]
[20] Physics Department, University of Lund, Lund, Sweden[g]
[21] Physics Department, University of Manchester, Manchester, UK[b]
[22] CPPM, CNRS/IN2P3 - Univ Mediterranee, Marseille - France
[23] Institute for Theoretical and Experimental Physics, Moscow, Russia[l]
[24] Lebedev Physical Institute, Moscow, Russia[e,h]
[25] Max-Planck-Institut für Physik, München, Germany
[26] LAL, Université de Paris-Sud, IN2P3-CNRS, Orsay, France
[27] LPNHE, Ecole Polytechnique, IN2P3-CNRS, Palaiseau, France
[28] LPNHE, Universités Paris VI and VII, IN2P3-CNRS, Paris, France
[29] Institute of Physics, Academy of Sciences of the Czech Republic, Praha, Czech Republic[e,i]
[30] Faculty of Mathematics and Physics, Charles University, Praha, Czech Republic[e,i]
[31] Dipartimento di Fisica Università di Roma Tre and INFN Roma 3, Roma, Italy
[32] Paul Scherrer Institut, Villigen, Switzerland
[33] Fachbereich Physik, Bergische Universität Gesamthochschule Wuppertal, Wuppertal, Germany

[34] *Yerevan Physics Institute, Yerevan, Armenia*
[35] *DESY, Zeuthen, Germany*
[36] *Institut für Teilchenphysik, ETH, Zürich, Switzerland[j]*
[37] *Physik-Institut der Universität Zürich, Zürich, Switzerland[j]*

[38] *Also at Physics Department, National Technical University, Zografou Campus, GR-15773 Athens, Greece*
[39] *Also at Rechenzentrum, Bergische Universität Gesamthochschule Wuppertal, Germany*
[40] *Also at Institut für Experimentelle Kernphysik, Universität Karlsruhe, Karlsruhe, Germany*
[41] *Also at Dept. Fis. Ap. CINVESTAV, Mérida, Yucatán, México[k]*
[42] *Also at University of P.J. Šafárik, Košice, Slovak Republic*
[43] *Also at CERN, Geneva, Switzerland*
[44] *Also at Dept. Fis. CINVESTAV, México City, México[k]*

1 Introduction

The observation of events with a large rapidity gap in the distribution of the final state hadrons at HERA [1] allows the nature of colour singlet exchange in strong interactions to be investigated. Colour singlet exchange interactions have been successfully modelled [2] in terms of phenomenological Regge theory [3] and, at high energy, are attributed to diffractive or pomeron exchange. HERA allows the partonic nature of diffraction to be investigated in deep–inelastic scattering (DIS) using the virtual photon as a probe.

The inclusive diffractive DIS structure function F_2^D is directly sensitive to the quark content of the diffractive exchange [4,5]. Information about the gluon content can be inferred indirectly from scaling violations. However, the measurement of the hadronic final state in diffraction gives further, more direct, information about the gluon content [6–9]. The production of open charm is expected to be particularly sensitive to the gluon content because studies in inclusive DIS reveal that the dominant contribution comes from the boson–gluon–fusion (BGF) mechanism [10]. The presence of the hard scale, provided by the charm quark mass, allows a variety of perturbative QCD-based models of diffraction to be tested.

This article describes the measurement of diffractive open charm production in DIS at HERA, which was performed using the H1 detector. Measurements of the total $D^{*\pm}$ cross section and of differential distributions which explore the dynamics of diffractive charm production are presented. The ratio of the diffractive $D^{*\pm}$ cross section to the inclusive $D^{*\pm}$ cross section is also measured.

The paper is organised as follows. The kinematics of diffractive DIS are introduced in section 2. The different theoretical approaches to diffractive charm production are summarised in section 3. In section 4, the H1 detector, the data selection, the cross section measurement procedure and the evaluation of the systematic uncertainties are explained. The results, in the form of the total and differential cross sections are presented and discussed in section 5.

2 Kinematics

The process studied in this paper is $ep \rightarrow eXY \rightarrow e(D^{*\pm}X')Y$ and is shown in figure 1. The electron produces a virtual photon γ^* (with four–momentum q) which interacts with the proton (with four–momentum P). If the interaction takes place via colour singlet exchange, the photon and proton dissociate into two distinct hadronic systems X and Y, with invariant masses M_X and M_Y, respectively. The system Y is that which is closest to the outgoing proton direction. In the case where M_X and M_Y are small compared with the photon-proton centre of mass energy W, the two systems are separated by a large rapidity gap. In addition to the standard DIS kinematic variables Q^2, y and Bjorken x the following variables are defined

$$x_{I\!\!P} = \frac{q \cdot (P - p_Y)}{q \cdot P} \; ; \qquad t = (P - p_Y)^2 \; ; \qquad \beta = \frac{Q^2}{2q \cdot (P - p_Y)} = \frac{x}{x_{I\!\!P}}, \qquad (1)$$

where p_Y is the four–momentum of Y. The quantity $x_{I\!\!P}$ may be interpreted as the longitudinal momentum fraction, with respect to the incoming proton, of the colourless exchange and t is
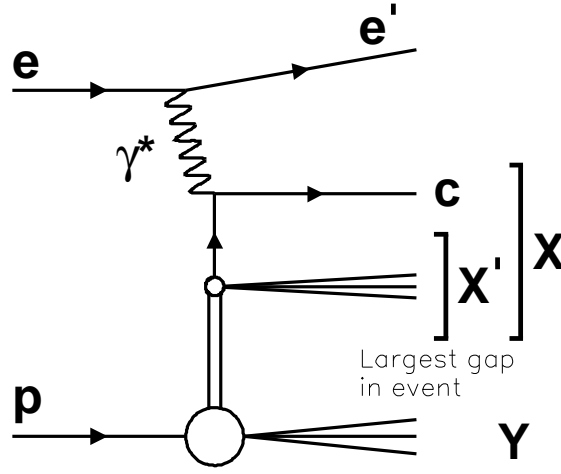
4

Figure 1: *The process under study in this article is $ep \to eXY \to e(D^{*\pm}X')Y$. The electron ($e$) couples to a photon ($\gamma^\star$) which interacts with the proton (p) via colour singlet exchange, producing two distinct final state hadronic systems X and Y. The systems X and Y are separated by the largest gap in rapidity in the final state hadrons.*

the squared four–momentum transferred at the proton vertex. In the analysis presented in this paper, t and M_Y are constrained to be small by the experimental selection and are integrated over implicitly.

In a QCD interpretation in which a partonic structure is ascribed to the colourless exchange the lowest order (i.e. $\mathcal{O}(\alpha_s^0)$) contribution to the diffractive cross section in the proton infinite momentum frame is quark scattering ($\gamma^\star q \to q$). In this case β can be interpreted as the fractional longitudinal momentum of the exchange carried by the struck quark. The $\mathcal{O}(\alpha_s)$ contributions are the BGF ($\gamma^\star g \to q\bar{q}$) and QCD-Compton ($\gamma^\star q \to qg$) processes. In the $\mathcal{O}(\alpha_s)$ case the invariant mass squared $\hat{s}$ of the partons emerging from the hard subprocess is non-zero. Therefore, the quantity $z_{I\!\!P}$ is introduced

$$z_{I\!\!P} = \beta \cdot \left(1 + \frac{\hat{s}}{Q^2}\right) \tag{2}$$

which corresponds to the longitudinal momentum fraction of the colourless exchange carried by the parton (quark or gluon) which enters the hard interaction.

3 Models of Diffractive $D^{*\pm}$ Production

A detailed description of the models used in this paper is given in [9]. A brief summary focusing on the production of open charm in each of the models is given here. For ease of comparison with the data in this paper the models are divided into three groups: the 'resolved pomeron' model, '2-gluon exchange' models and 'soft colour neutralisation' models.

In the 'resolved pomeron' model [11] the diffractive cross section factorises into deep–inelastic scattering from the pomeron and a pomeron flux factor, motivated by Regge theory,

which describes the probability for finding a pomeron in the proton. Within this picture, the partonic content of the pomeron has been determined by QCD analyses of HERA diffractive data [4, 12]. The parton distributions, obtained from fits to the data, contain a dominant gluon distribution. Open charm is produced in the resolved pomeron model by the BGF process, where the photon interacts with a gluon of the pomeron carrying a fraction $z_{I\!\!P}$ of the pomeron longitudinal momentum.

In '2-gluon exchange' models diffractive DIS is studied in the proton rest frame by considering $q\bar{q}$ and $q\bar{q}g$ photon fluctuations as colour dipoles scattering off the proton. Open charm can be produced when the photon fluctuates into $c\bar{c}$ or $c\bar{c}g$ states. The simplest realisation of net colour singlet exchange between these partonic fluctuations and the proton at the parton level is a pair of gluons with opposite colour [13]. In perturbative QCD, the cross section for 2-gluon exchange is related to the square of the k_T–unintegrated gluon density of the proton $\mathcal{F}(x, k_T^2)$ [14, 15], where k_T is the parton transverse momentum relative to the proton direction. In the 'saturation' model [16] the calculation of the $q\bar{q}g$ cross section is made under the assumption of strong k_T ordering of the final state partons, where $k_T^{(g)} \ll k_T^{(q,\bar{q})}$. In an alternative approach [17, 18] (hereafter referred to as 'BJLW') the calculation of the $q\bar{q}g$ final state includes configurations without strong k_T ordering. In this model all outgoing partons are required to have high k_T and the minimum value for the final state gluon transverse momentum $k_{T,g}^{cut}$ is a free parameter which can be tuned to describe the data. The 2-gluon exchange calculations are performed under the assumption of low $x_{I\!\!P}$ ($x_{I\!\!P} < 0.01$) to avoid contributions from secondary reggeon exchanges which correspond to quark exchange in the models.

In 'soft colour neutralisation' models an alternative approach to diffractive DIS is given which leads to very similar properties of inclusive and diffractive DIS final states. In the soft colour interaction model (SCI) [19], open charm is produced via BGF from the gluon distribution of the proton. It is then assumed that the partons produced in the hard interactions can exchange soft gluons with the background colour field of the incoming proton leaving all momenta unchanged. Large rapidity gap events may be produced this way when the soft interactions lead to a net colour singlet exchange. The probability for soft colour exchange is assumed to be independent of the kinematics of the hard scattering process.

The generalised area law (GAL) [20] approach is a modification of the Lund String model [21]. The production mechanism for open charm is similar to that in the SCI model except that it is formulated in terms of interactions between the colour strings connecting the partons in an event. In this model the probability for a soft colour interaction is not constant but is exponentially suppressed by the difference between the areas in momentum space spanned by the strings before and after the colour rearrangement.

The 'semi-classical' model [22] is a non-perturbative model based on the dipole approach. In the proton rest frame the photon fluctuations scatter off a superposition of soft colour fields representing the proton. In this approach, the $q\bar{q}g$ fluctuation is expected to be dominant for open charm production [23]. If the gluon is the lowest k_T parton, then the contribution can be related to BGF in the proton infinite momentum frame.

Comparison of the data with the 'resolved pomeron', the '2-gluon exchange' and the 'semi-classical' models is facilitated by their implementation within the RAPGAP Monte Carlo generator [24]. The predictions of the SCI and GAL models are calculated using the AROMA

Monte Carlo generator [25]. The cross section predictions in this article are all calculated assuming a charm quark mass $m_c = 1.5$ GeV. For the hadronisation fraction $f(c \rightarrow D^{*\pm})$ the value $0.233 \pm 0.010 \pm 0.011$ [26] is used. The momentum fraction of the charm quark carried by the $D^{*\pm}$ is calculated using the Peterson *et al.* model [27] with the fragmentation parameter $\epsilon = 0.078$.

4 Experimental Procedure

The data presented in this analysis were collected over the years 1996 and 1997, when HERA collided positrons with energy $E_e = 27.5$ GeV with protons of energy $E_p = 820$ GeV. Requiring all essential detector components to be operational the available integrated luminosity is $19.1\mathrm{pb}^{-1}$. Further details of this analysis beyond those given here can be found in [28].

4.1 The H1 Detector

A short overview of the detector components most relevant for the present analysis is given here. A detailed description of the H1 detector can be found in [29]. The z–axis of the H1 detector is taken along the beam direction such that positive z values refer to the direction of the outgoing proton beam, referred to as the 'forward' direction.

Charged particles emerging from the interaction region are measured by the central tracking device (CTD) in the range $-1.5 < \eta < 1.5^1$. The CTD comprises two large cylindrical central jet drift chambers (CJC) and two z chambers situated concentrically around the beam-line within a solenoidal magnetic field of 1.15 T. The resolution achieved by the CTD is $\sigma(p_T)/p_T \simeq 0.01 p_T/\mathrm{GeV}$. The CTD also provides triggering information based on track segments in the $r - \phi$ plane from the CJC and the position of the vertex using a double layer of multi-wire proportional chambers (MWPC). The energies of final state particles are measured in the Liquid Argon (LAr) calorimeter which surrounds the tracking chambers and covers the range $-1.5 < \eta < 3.4$. The backward region ($-4.0 < \eta < -1.4$) is covered by a lead–scintillating fibre calorimeter (SPACAL [30]) with electromagnetic and hadronic sections. In front of the SPACAL, the Backward Drift Chamber (BDC) [31] provides track segments of charged particles.

Detectors close to the beam pipe in the direction of the outgoing proton are used in the selection of large rapidity gap events. These are the Forward Muon Detector (FMD), the Proton Remnant Tagger (PRT) and the Plug calorimeter (PLUG). The FMD is located at $z = 6.5$ m and covers the pseudorapidity range $1.9 < \eta < 3.7$ directly. The PLUG allows energy measurements to be made over the range $3.5 < \eta < 5.5$. Particles produced at larger η can also be detected because of secondary scattering with the beam-pipe. The PRT, a set of scintillators surrounding the beam pipe at $z = 26$ m, can tag hadrons in the region $6.0 \lesssim \eta \lesssim 7.5$.

---

[1]The pseudorapidity η of an object detected with polar angle θ is defined as $\eta = -\ln \tan(\theta/2)$.

4.2   Event Selection

The events were triggered by an electromagnetic energy cluster in the SPACAL, in coincidence with a charged track signal from both the MWPC and the CJC. The positrons are identified in the SPACAL as clusters with energy $E'_e > 9$ GeV which have properties consistent with electromagnetic deposition, and for which the centre of gravity of the cluster matches a charged track segment in the BDC to within 2.5 cm. The selected events are also required to have a reconstructed vertex from the CTD within ± 35 cm of the nominal vertex. In order to suppress events with initial state photon radiation the summed $E - p_z$ of the event calculated using all reconstructed final state particles, including the positron, is required to be greater than 35 GeV. The kinematic region covered by the measurement is $2 < Q^2 < 100$ GeV^2 and $0.05 < y < 0.7$. To minimise the correction due to QED radiative effects, Q^2, y and x are reconstructed from the energy and angle θ' of the scattered positron and the hadronic final state using the 'Σ method' [32].

Diffractive events are selected experimentally by the absence of activity in the outgoing proton region. No signal above noise thresholds is allowed in the FMD, the PRT, the PLUG and the most forward part ($\eta > 3.3$) of the LAr calorimeter. This ensures that there is a large rapidity gap covering at least $3.3 < \eta \leq 7.5$ between the photon dissociation system X and the proton remnant system Y. Monte Carlo studies show that the absence of particles in the detectors close to the beam pipe restricts the mass of the proton remnant system to $M_Y < 1.6$ GeV and the momentum transfer to the proton to $|t| < 1$ GeV^2.

The four–momentum of the system X, which is well contained in the central detector, is reconstructed using information from the LAr and SPACAL calorimeters together with the CJC [33]. The variable $x_{I\!P}$ is calculated from

$$x_{I\!P} = \frac{\sum_{X+e'}(E + p_z)}{2E_p} \tag{3}$$

where E and p_z are the energy and longitudinal momentum of each final state particle in the laboratory frame, and the sum runs over the scattered positron e' and all detected particles in the photon dissociation system X. The quantity β is calculated from $\beta = x/x_{I\!P}$. The cross section is restricted to the range $x_{I\!P} < 0.04$ to suppress contributions from non-diffractive scattering and secondary reggeon exchanges.

In this paper an hadronic observable $z_{I\!P}^{obs}$ is constructed which is analogous to x_g^{obs} for inclusive $D^{*\pm}$ production which was measured in [34]. In the resolved pomeron picture $z_{I\!P}^{obs}$ is an approximation to the momentum fraction $z_{I\!P}$ of the pomeron carried by the interacting gluon (see equation 2). The observable $z_{I\!P}^{obs}$ is defined as

$$z_{I\!P}^{obs} = \frac{M_{c\bar{c}}^2 + Q^2}{M_X^2 + Q^2}. \tag{4}$$

where $M_{c\bar{c}}^2$ is a hadron level estimate of $\hat{s}$ which is constructed from the scattered positron and the $D^{*\pm}$ meson in an identical manner to that used for the gluon momentum fraction x_g^{obs} in [34]. Monte Carlo simulations show that the resolution in the hadronic variable $z_{I\!P}^{obs}$ is approximately 30%, and that there is a good correlation between $z_{I\!P}^{obs}$ and $z_{I\!P}$ as calculated from the kinematics of the outgoing partons. The variable $z_{I\!P}^{obs}$ can be interpreted as the fraction of the energy of the system X which is carried by the $c\bar{c}$ pair emerging from the hard scattering.

8

4.3 Reconstruction of $D^{*\pm}$ Mesons

The $D^{*\pm}$ mesons are reconstructed using the $D^{*\pm} - D^0$ mass difference method [35] in the decay channel

$$D^{*\pm} \to D^0 \, \pi^+_{slow} \to (K^- \, \pi^+) \, \pi^+_{slow} \, (+c.c.), \tag{5}$$

which has a branching fraction of 2.59% [36]. The reconstruction method is detailed in [37]. The decay products are detected in the CTD and are required to have a transverse momentum p_T of at least 140 MeV for the π_{slow} and 250 MeV for both the K and π.
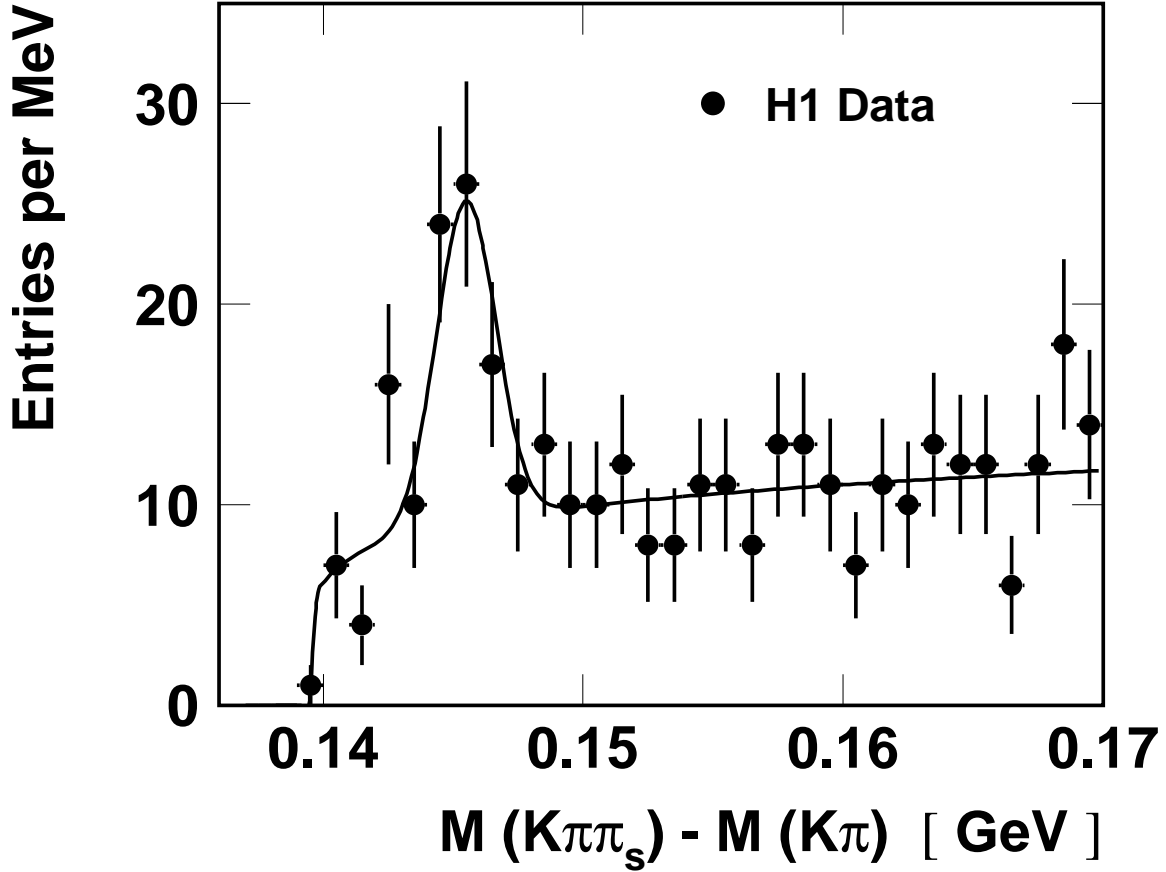

Figure 2: *Distribution of the mass difference* $\Delta M = M(K^\mp \pi^\pm \pi^\pm_{slow}) - M(K^\mp \pi^\pm)$, *with a curve fitted to the form* $a(\Delta M - M_\pi)^b +$ *Gaussian.*

The invariant mass of the $K\pi$ combination has to be consistent with the D^0 mass within ± 80 MeV. After cuts on the direction ($|\eta(K\pi\pi)| < 1.5$) and transverse momentum ($p_T(K\pi\pi) > 2$ GeV), the mass difference distribution $\Delta M = M(K\pi\pi_{slow}) - M(K\pi)$ is plotted in figure 2. The number of $D^{*\pm}$ candidates is determined by fitting the histogram in figure 2 with a Gaussian distribution for the signal plus a background function $a(\Delta M - M_\pi)^b$, where M_π denotes the

9

mass of the pion. The position and width of the Gaussian are fixed to values taken from a higher statistics sample of events where no diffractive cuts were applied [37]. The normalisation of the Gaussian and the background parameters a and b are allowed to vary. The resulting number of detected $D^{*\pm}$ mesons is 46 ± 10.

4.4 Cross Section Measurement

Monte Carlo simulations are used to correct the data for the effects of losses and migrations due to the finite resolution of the H1 detector. The efficiency is calculated by running the H1 detector simulation program on a sample of $D^{*\pm}$ events from the diffractive Monte Carlo generator RAPGAP [24] in the resolved pomeron mode with the t dependence of the cross section parameterised as $e^{-6|t|}$. The RAPGAP program is used to model events which contain an elastic proton ($M_Y = m_p$) in the kinematic range $x_{I\!P} < 0.1$. Migrations from $x_{I\!P} > 0.1$ or from large values of M_Y ($M_Y > 5$ GeV) are modelled by using a simulation of the heavy quark generator AROMA [25] in the inclusive mode. The contribution is of the order 5% to the selected sample of events. An additional correction of $-8\% \pm 6\%$ is applied to account for the net smearing across the $M_Y = 1.6$ GeV boundary. Since only elastically scattered protons have been simulated in RAPGAP, this correction is evaluated using the proton dissociation simulation in the DIFFVM [38] generator[2]. A further correction of $+4\% \pm 1\%$ takes into account diffractive events rejected due to fluctuations in the noise level in the FMD. This correction is estimated directly from the data, using a sample of randomly selected events, not correlated with a physics trigger. An additional source of background is the contribution of reflections in the D^0 mass window, coming from D^0 channels other than that defined in equation 5. They are estimated, from simulations using the AROMA Monte Carlo, to be 3.5% [28]. The contribution from photoproduction background is found to be negligible. QED radiative corrections were calculated to be approximately 2% using the RAPGAP program interfaced to HERACLES [39].

4.5 Systematic Uncertainties

The following sources of systematic error are taken into account

- The uncertainty in the physics model for $D^{*\pm}$ production used to compute the efficiency corrections is estimated by varying the shapes of the kinematic distributions in the simulations beyond the limits imposed by previous measurements or the present data. This is done by reweighting the $x_{I\!P}$ distribution to that observed in data; the β distribution by $(1 \pm 0.3\beta)$ and the t distribution by $e^{\pm 2t}$. The resulting systematic uncertainties on the cross section measurements range between 10% and 20% with the largest contribution originating from the variation of the $x_{I\!P}$ distribution. The uncertainties are verified using simulations of models with different underlying kinematic distributions.

- The total uncertainty due to the reconstruction efficiency, mass and momentum resolution of the central tracker for the three tracks was estimated in the analysis of the inclusive DIS $D^{*\pm}$ cross section to be $^{+9\%}_{-4\%}$ [37].

---

[2]For the correction, it is assumed that the ratio of diffractive proton elastic to diffractive proton dissociative interactions is $1 : 1$.

- An error of 8% is found by varying the details of the fitting procedure used to obtain the number of $D^{*\pm}$ mesons.

- The uncertainty in the correction due to the smearing of events across the boundary $M_Y = 1.6$ GeV is estimated by varying in the DIFFVM simulation: the efficiency of the forward detectors, the assumed M_Y distribution, the ratio of double to single dissociation between 0.5 and 2 and the assumed t dependence for double dissociation. This contributes 6% to the systematic error.

- The uncertainty in the trigger efficiency gives a contribution of 5% to the systematic error.

- The uncertainty due to the assumed charm fragmentation scheme is estimated by using parameterisations of the Peterson model and the standard Lund string model in JETSET [21]. This leads to an average uncertainty of 5% in the cross sections.

- The uncertainty in the correction due to QED radiative effects is estimated as 3%.

- The number of events migrating into the sample from $x_{I\!\!P} > 0.1$ or $M_Y > 5$ GeV is varied by $\pm 50\%$, leading to an average systematic error of 3%.

  Other sources of systematic error are the uncertainty in the measured energy and angle of the scattered positron, uncertainties in the hadronic energy scale of the liquid argon and SPACAL calorimeters, the uncertainty in the luminosity measurement, the uncertainty on the fraction of events lost due to noise in the FMD and the uncertainty in the branching ratio for the measured decay channel. Each of them is responsible for an error of no more than 2.5%.

The total systematic error for each point has been obtained by adding all individual contributions in quadrature. It ranges between 20% and 30% and for most data points is similar in magnitude to the statistical error.

5   Results

The total $D^{*\pm}$ production cross section for the kinematic region $2 < Q^2 < 100$ GeV^2, $0.05 < y < 0.7$, $x_{I\!\!P} < 0.04$, $M_Y < 1.6$ GeV, $|t| < 1$ GeV^2, $p_{T,D^*} > 2$ GeV and $|\eta_{D^*}| < 1.5$ is

$$\sigma(ep \to e(D^{*\pm}X')Y) = 246 \pm 54 \text{ (stat.)} \pm 56 \text{ (syst.) pb} . \tag{6}$$

The ratio of the diffractive $D^{*\pm}$ cross section to the inclusive $D^{*\pm}$ cross section measured in the same kinematic range defined in terms of Q^2, y, p_{T,D^*} and η_{D^*} is found to be

$$5.9 \pm 1.1 \text{ (stat.)} \pm 1.1 \text{ (syst.)}\%, \tag{7}$$

where the inclusive $D^{*\pm}$ cross section has been determined as in [37]. The error in the ratio is dominated by the uncertainties pertaining to the measurement of the diffractive cross section.

11

Model		cross section (pb)
resolved	H1 fit 2	368
pomeron	H1 fit 3	433
	ACTW fit D	481
soft colour	SCI	203
neutralisation	GAL	328
	semi-classical	196
H1 Data		246 ± 54 (stat.) ± 56 (syst.) pb

Table 1: *The predictions for the total diffractive $D^{*\pm}$ cross section for two groups of models: the resolved pomeron and soft colour neutralisation approaches. The bottom row shows the cross section measured in the data.*

In table 1 the total cross section is compared with some of the phenomenological models discussed in section 3. The first three rows of table 1 show the predictions for the cross section for three different sets of parton parameterisations within the resolved pomeron model. The first two predictions are based on the parton distributions of the pomeron and sub-leading exchange from the leading order DGLAP analysis of F_2^D from H1 [4]. The 'ACTW fit D' parameterisation is the best combined fit in [12] to H1 and ZEUS F_2^D data and ZEUS diffractive dijet data. All three sets of parton parameterisations give acceptable descriptions of F_2^D. All of the predictions using the three parton parameterisations exceed the data although the parameterisation with the flat gluon distribution ('H1 fit 2') is closest. The predictions shown are calculated with the factorisation and renormalisation scales set to $\mu^2 \equiv \mu_f^2 \equiv \mu_r^2 = Q^2 + p_T^2 + 4m_c^2$. Changing this scale to $p_T^2 + 4m_c^2$ produces an increase of around 20% in the predicted cross sections. Similarly, the variation of the charm quark mass by ± 0.1 GeV leads to an uncertainty of $\mp 10\%$ in the cross sections. Changing ϵ in the Peterson model from 0.078 to 0.035 and to 0.1 produces an uncertainty in the cross section predictions of $^{+15}_{-5}\%$. The values shown in the table are calculated with $\Lambda_{QCD} = 0.20$ GeV and the number of active quark flavours in the first order expression for α_s is $N_f = 4$. Selecting $\Lambda_{QCD} = 0.25$ GeV and $N_f = 5$ leads to an increase of about 10% in the cross sections. The contribution of $D^{*\pm}$ production from meson exchange in the predictions is less than 7%.

The cross section predictions from the semi-classical, SCI and GAL models are also shown in table 1 and are in agreement with the data. However, none of these models can simultaneously reproduce the shapes and normalisations of the differential dijet cross sections [9]. The semi-classical model prediction was calculated using the same factorisation scale as for the resolved pomeron model. The SCI and GAL model predictions use $\mu^2 = Q^2 + 2p_T^2 + 2m_c^2$. For each of the three models, the uncertainty in the predictions due to the variation of the factorisation scale, m_c and ϵ are similar to those for the resolved pomeron model.

Differential cross sections are shown in figures 3 and 4. They represent average values over the intervals shown in the figures.

In figure 3 the cross section is shown as a function of $x_{I\!P}$, $\log_{10} \beta$ and $z_{I\!P}^{obs}$ and compared to the QCD-based models described in section 3. The cross sections differential in $x_{I\!P}$ and $\log_{10} \beta$ are flat within experimental errors. Figure 3 shows that about 60% of charm production is in the region $z_{I\!P}^{obs} < 0.2$ where the contribution of the BGF process is expected to dominate.
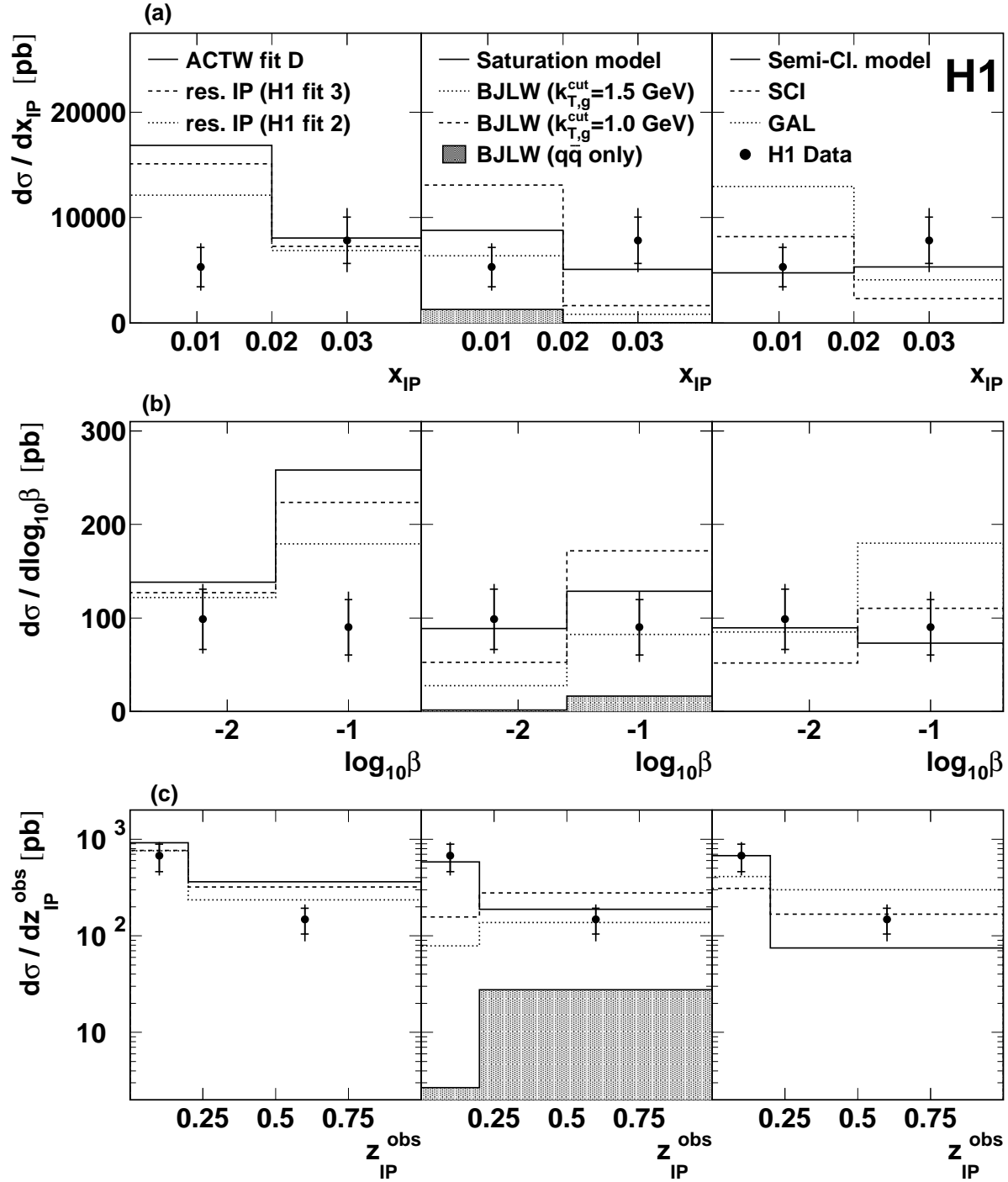
12

Figure 3: *Cross sections* $\sigma(ep \rightarrow e(D^{*\pm}X')Y)$ *as a function of (a)* $x_{I\!P}$*; (b)* $\log_{10} \beta$ *and (c)* $z_{I\!P}^{obs}$*. The data are points with error bars (inner: statistical, outer: total). Each distribution is plotted three times to allow comparison with the three groups of models described in the text.*
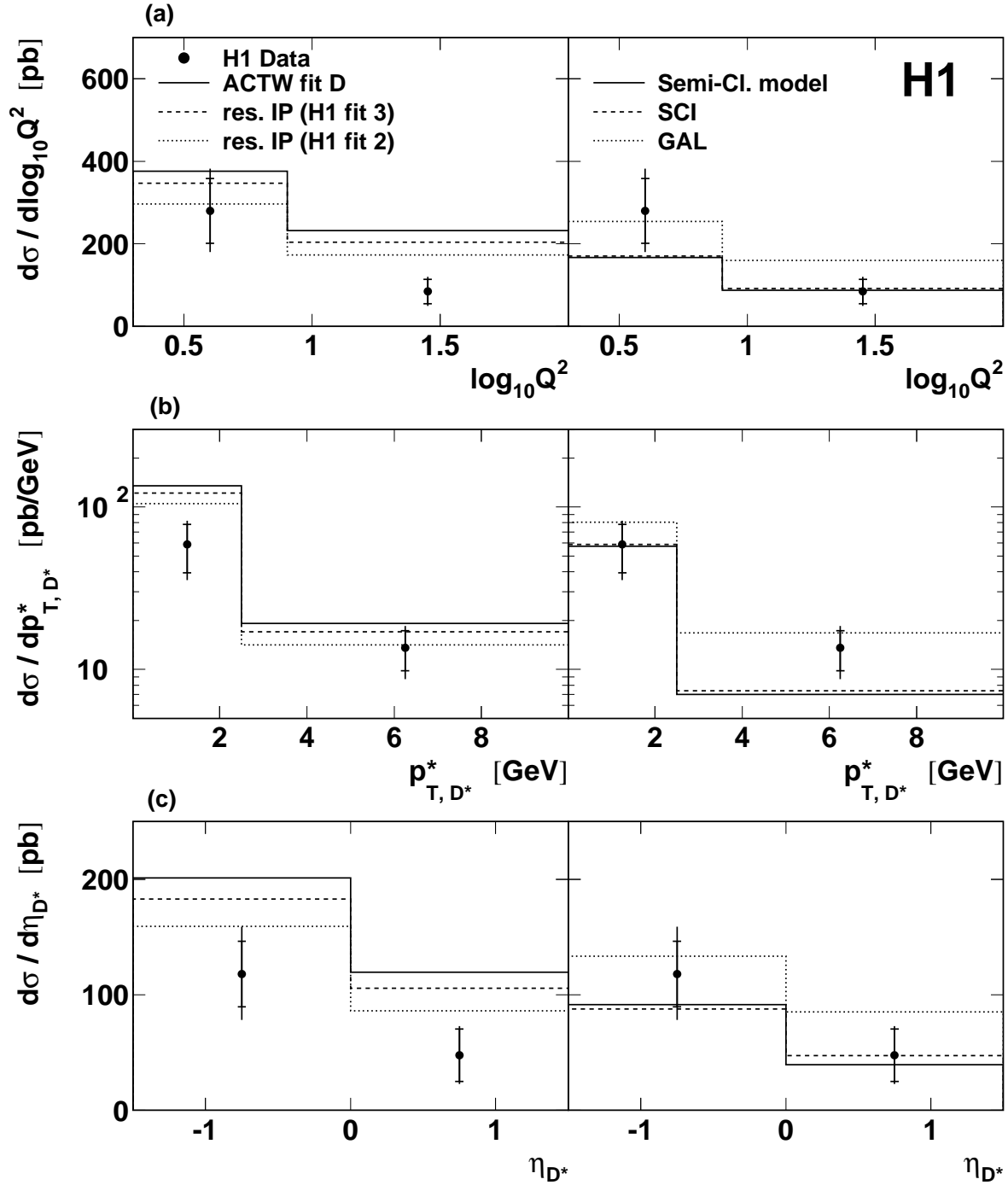
Figure 4: *Cross sections* $\sigma(ep \to e(D^{*\pm}X')Y)$ *as a function of (a)* $log_{10}Q^2$*; (b)* p^*_{T,D^*} *and (c)* η_{D^*}*. The data are points with error bars (inner: statistical, outer: total). Each distribution is plotted twice to allow comparison with two of the groups of models described in the text.*

The discrepancy between the resolved pomeron model predictions and the data is pronounced in the low $x_{I\!\!P}$, high β and high $z_{I\!\!P}^{obs}$ regions which are all correlated with low values of M_X. Of the three parton parameterisations the calculations which use 'H1 Fit 2' are shown to come closest to the data in this region. All three parameterisations are consistent with the data in the high M_X region.

The two gluon exchange models, directly applicable in the low $x_{I\!\!P}$ region ($x_{I\!\!P} < 0.01$) are also compared to the data in figure 3. The sensitivity of this measurement to the value of the transverse momentum cut-off $k_{T,g}^{cut}$ of the gluon in the $q\bar{q}g$ state within the BJLW model is also studied. Calculations which use cut-off values of 1.0 GeV and 1.5 GeV both give a fair description of the data in the low M_X region (i.e. the low $x_{I\!\!P}$, high β, high $z_{I\!\!P}^{obs}$ domain). These data also offer sensitivity to the relative contribution of the scattering of the $q\bar{q}$ fluctuation, which is shown as a shaded zone, and forms a sizeable component of the total two gluon exchange cross section. The saturation model reproduces reasonably well the normalisation of the data in the low $x_{I\!\!P}$ range, in which it is expected to be applicable, but also provides a good description of the data in the remaining region of phase space.

The semi-classical model gives a good description of the distributions shown in figure 3. Both the SCI and GAL models provide a satisfactory description of the spectra although the GAL model tends to overestimate the data in the low M_X domain.

In figure 4, the $D^{*\pm}$ cross section is plotted differentially at 2 values of $\log_{10} Q^2$, p^*_{T,D^*} and η_{D^*}, where p^*_{T,D^*} is the transverse momentum of the $D^{*\pm}$ in the $\gamma^* p$ centre of mass system. The data tend to fall off with higher values of each of these variables.

Since these distributions are integrated over the full $x_{I\!\!P}$ range of this measurement, a comparison is made only with resolved pomeron calculations and soft colour neutralisation models. Both sets of models provide a reasonable description of the data.

6   Conclusion

The dynamics of open diffractive charm production in DIS have been studied for the first time at HERA. The total $D^{*\pm}$ production cross section in the kinematic range $2 < Q^2 < 100$ GeV^2, $0.05 < y < 0.7$, $x_{I\!\!P} < 0.04$, $M_Y < 1.6$ GeV, $|t| < 1$ GeV^2, $p_{T,D^*} > 2$ GeV and $|\eta_{D^*}| < 1.5$ has been found to be 246 ± 54 (stat.) ± 56 (syst.) pb. In the studied region about 6% of the total $D^{*\pm}$ cross section is produced diffractively.

The cross section has been measured as a function of $x_{I\!\!P}$, $\log_{10} \beta$, $z_{I\!\!P}^{obs}$, $\log_{10} Q^2$, p^*_{T,D^*} and η_{D^*}. The data show a sizeable component of charm production in the low $z_{I\!\!P}^{obs}$ region which is suggestive of the dominance of the contribution from the boson–gluon–fusion process.

A number of QCD-based models which give a good description of the inclusive diffractive cross section were compared with the measurement. A reasonable description of the data is provided by a model based on the resolved pomeron picture using various assumptions for the partonic composition of the colourless exchange. A parton parameterisation containing a flat gluon dependence ('H1 Fit 2') comes closest to the data. Predictions of two gluon exchange processes were found to match the data in the low $x_{I\!\!P}$ region. Soft colour neutralisation models give a satisfactory description of the data.

Acknowledgements

References

[1] M. Derrick *et al.* [ZEUS Collaboration], Phys. Lett. B **315** (1993) 481;
    T. Ahmed *et al.* [H1 Collaboration], Nucl. Phys. B **429** (1994) 477.

[2] P. D. Collins, "An Introduction To Regge Theory And High-Energy Physics," *Cambridge 1977, 445p*.

[3] T. Regge, Nuovo Cim. **14** (1959) 951;
    T. Regge, Nuovo Cim. **18** (1960) 947.

[4] C. Adloff *et al.* [H1 Collaboration], Z. Phys. C **76** (1997) 613 [hep-ex/9708016].

[5] J. Breitweg *et al.* [ZEUS Collaboration], Eur. Phys. J. C **1** (1998) 81 [hep-ex/9709021];
    J. Breitweg *et al.* [ZEUS Collaboration], Eur. Phys. J. C **6** (1999) 43 [hep-ex/9807010].

[6] C. Adloff *et al.* [H1 Collaboration], Eur. Phys. J. C **1** (1998) 495 [hep-ex/9711006];
    C. Adloff *et al.* [H1 Collaboration], Eur. Phys. J. C **5** (1998) 439 [hep-ex/9804012];
    C. Adloff *et al.* [H1 Collaboration], Phys. Lett. B **428** (1998) 206 [hep-ex/9803032].

[7] J. Breitweg *et al.* [ZEUS Collaboration], Phys. Lett. B **421** (1998) 368 [hep-ex/9710027].

[8] J. Breitweg *et al.* [ZEUS Collaboration], Eur. Phys. J. C **5** (1998) 41 [hep-ex/9804013];
    C. Adloff *et al.* [H1 Collaboration], Eur. Phys. J. C **6** (1999) 421 [hep-ex/9808013].

[9] C. Adloff *et al.* [H1 Collaboration], Eur. Phys. J. C **20** (2001) 29 [hep-ex/0012051].

[10] C. Adloff *et al.* [H1 Collaboration], Z. Phys. C **72** (1996) 593 [hep-ex/9607012];
    J. Breitweg *et al.* [ZEUS Collaboration], Phys. Lett. B **407** (1997) 402 [hep-ex/9706009].

[11] G. Ingelman and P. E. Schlein, Phys. Lett. B **152** (1985) 256.

[12] L. Alvero, J. C. Collins, J. Terron and J. J. Whitmore, Phys. Rev. D **59** (1999) 074022 [hep-ph/9805268];
    L. Alvero, J. C. Collins and J. J. Whitmore, hep-ph/9806340.

[13] F. E. Low, Phys. Rev. D **12** (1975) 163;
    S. Nussinov, Phys. Rev. Lett. **34** (1975) 1286.

[14] E. A. Kuraev, L. N. Lipatov and V. S. Fadin, Sov. Phys. JETP **45** (1977) 199 [Zh. Eksp. Teor. Fiz. **72** (1977) 377];
I. I. Balitsky and L. N. Lipatov, Sov. J. Nucl. Phys. **28** (1978) 822 [Yad. Fiz. **28** (1978) 1597];
L. N. Lipatov, Sov. Phys. JETP **63** (1986) 904 [Zh. Eksp. Teor. Fiz. **90** (1986) 1536].

[15] S. Catani, M. Ciafaloni and F. Hautmann, Nucl. Phys. B **366** (1991) 135.

[16] K. Golec-Biernat and M. Wüsthoff, Phys. Rev. D **59** (1999) 014017 [hep-ph/9807513];
K. Golec-Biernat and M. Wüsthoff, Phys. Rev. D **60** (1999) 114023 [hep-ph/9903358].

[17] J. Bartels, H. Lotter and M. Wüsthoff, Phys. Lett. B **379** (1996) 239 [Erratum-ibid. B **382** (1996) 449] [hep-ph/9602363];
J. Bartels, C. Ewerz, H. Lotter and M. Wüsthoff, Phys. Lett. B **386** (1996) 389 [hep-ph/9605356];
H. Lotter, Phys. Lett. B **406** (1997) 171 [hep-ph/9612415].

[18] J. Bartels, H. Jung and M. Wüsthoff, Eur. Phys. J. C **11** (1999) 111 [hep-ph/9903265];
J. Bartels, H. Jung and A. Kyrieleis, hep-ph/0010300 and DESY 01-116 to appear.

[19] A. Edin, G. Ingelman and J. Rathsman, Phys. Lett. B **366** (1996) 371 [hep-ph/9508386];
A. Edin, G. Ingelman and J. Rathsman, Z. Phys. C **75** (1997) 57 [hep-ph/9605281].

[20] J. Rathsman, Phys. Lett. B **452** (1999) 364 [hep-ph/9812423].

[21] T. Sjöstrand, Comput. Phys. Commun. **82** (1994) 74.

[22] W. Buchmüller, T. Gehrmann and A. Hebecker, Nucl. Phys. B **537** (1999) 477 [hep-ph/9808454].

[23] W. Buchmüller, M. F. McDermott and A. Hebecker, Phys. Lett. B **404** (1997) 353 [hep-ph/9703314].

[24] H. Jung, Comput. Phys. Commun. **86** (1995) 147;
(see also http://www.desy.de/~jung/rapgap.html)

[25] G. Ingelman, J. Rathsman and G. A. Schuler, Comput. Phys. Commun. **101** (1997) 135 [hep-ph/9605285].

[26] R. Barate *et al.* [ALEPH Collaboration], Eur. Phys. J. C **16** (2000) 597 [hep-ex/9909032].

[27] C. Peterson, D. Schlatter, I. Schmitt and P. Zerwas, Phys. Rev. D **27** (1983) 105.

[28] S. Hengstmann: *A Measurement of Diffractive Charm Production at HERA*, Ph.D. Thesis, University of Zürich (2000);
P. Thompson: *Open Charm Production in Inclusive and Diffractive Deep–Inelastic Scattering at HERA*, Ph.D. Thesis, University of Birmingham (1999);
Both available from http://www-h1.desy.de/publications/theses_list.html.

[29] I. Abt *et al.* [H1 Collaboration], Nucl. Instrum. Meth. A **386** (1997) 310 and 348.

[30] R. D. Appuhn *et al.* [H1 SPACAL Group Collaboration], Nucl. Instrum. Meth. A **386** (1997) 397.

[31] H1 collaboration, Technical proposal for the upgrade of the backward region of the H1 detector, DESY internal report PRC-93/02.

[32] U. Bassler and G. Bernardi, Nucl. Instrum. Meth. A **361** (1995) 197 [hep-ex/9412004].

[33] C. Adloff *et al.* [H1 Collaboration], Z. Phys. C **74** (1997) 221 [hep-ex/9702003].

[34] C. Adloff *et al.* [H1 Collaboration], Nucl. Phys. B **545** (1999) 21 [hep-ex/9812023].

[35] G. J. Feldman *et al.*, Phys. Rev. Lett. **38** (1977) 1313.

[36] D. E. Groom *et al.* [Particle Data Group Collaboration], Eur. Phys. J. C **15** (2000) 1.

[37] C. Adloff *et al.* [H1 Collaboration], *Measurement of $D^{*\pm}$ Meson Production and F_2^c in Deep Inelastic Scattering at HERA*, DESY 01-100, hep-ex/0108039, submitted to Phys. Lett. B.

[38] B. List: *Diffraktive J/ψ-Produktion in Elektron-Proton-Stößen am Speicherring HERA*, Diploma Thesis, Tech. Univ. Berlin (1993), unpublished;
B. List, A. Mastroberardino: *DIFFVM: A Monte Carlo Generator for diffractive processes in ep scattering* in *Monte Carlo Generators for HERA Physics*, A. Doyle, G. Grindhammer, G. Ingelman, H. Jung (eds.), DESY-PROC-1999-02 (1999) 396.

[39] A. Kwiatkowski, H. Spiesberger and H. J. Mohring, Comput. Phys. Commun. **69** (1992) 155.